Improved Performance of d31-Mode Needle-actuating Transducer with PMN-PT Piezocrystal

Jiang, Tingyi; Xia, Chunming; Cochran, Sandy; Huang, Zhihong

Published in:
IEEE Transactions on Ultrasonics, Ferroelectrics and Frequency Control

DOI:
10.1109/TUFFC.2018.2838566

Publication date:
2018

Document Version
Peer reviewed version

Improved Performance of d_{31}-Mode Needle-actuating Transducer with PMN-PT Piezocrystal

Tingyi Jiang[1], Chunming Xia[2], Sandy Cochran[3], Zhihong Huang[1]

[1]School of Science and Engineering, University of Dundee, Dundee, UK

[2]School of Mechanical and Power Engineering, East China University of Science and Technology, Shanghai, China

[3]School of Engineering, University of Glasgow, Glasgow, UK

***Abstract*—Prototypes of a PZT-based ultrasound needle-actuating device have shown the ability to reduce needle penetration force and enhance needle visibility with color Doppler imaging during needle insertion for tissue biopsy and regional anaesthesia. However, the demand for smaller, lighter devices and the need for high performance transducers have motivated investigation of a different configuration of needle actuation transducer, utilizing the d_{31}-mode of PZT4 piezoceramic, and exploration of further improvement in its performance using relaxor-type piezocrystal. This paper outlines the development of the d_{31}-mode needle actuation transducer design from simulation to fabrication and demonstration. Full characterization was performed on transducers for performance comparison. The performance of the proposed smaller, lighter d_{31}-mode transducer is comparable with previous d_{33}-mode transducers. Furthermore, it has been found to be much more efficient when using PMN-PT piezocrystal rather than piezoceramic.**

Keywords--- Needle; Needle-actuating device; Transducer; Piezocrystal; d_{31} mode

I. INTRODUCTION

Ultrasound-enhanced operation is used in many different medical applications, including dental cleaning, tissue dissection and high intensity focused ultrasound [1-3]. For example, ultrasound actuation of surgical instruments for biological tissue dissection, ablation and fragmentation has shown the advantages in excellent haemostasis, more accurate cutting and less thermal damage than conventional high frequency electro-scalpels [4]. Recently, ultrasound-actuated needle devices for tissue biopsy and regional anaesthesia have emerged as further potential medical applications and researchers have demonstrated their ability to reduce the needle penetration force and enhance needle visibility with color Doppler ultrasound imaging [5].

To date, the ultrasound needle-actuation transducers in these devices have been based on the mass-spring configuration, which is clumsy and complicated to manufacture at the small scale required [6]. Although other kinds of needle-actuation devices with simple design exist, they are not working at ultrasonic frequency and most of them need some modifications on the standard needle [7, 8]. Small, simple and lightweight ultrasonic devices with high performance and low spatial volume are preferred in the medical industry. This led us to investigate the potential use of piezocrystals since these recently-developed piezoelectric materials show great potential to supersede traditional piezoceramics in a range of applications, mainly because of their high strain and coupling coefficients [9-11]. However, the pressure-sensitive nature of piezocrystals [12] limits their use in mass-spring transducers in the needle-actuation application because prestress up to 40 MPa is needed [13]. Researchers have reported variation of key properties with pressure up to 60 MPa with the coupling coefficient, k_t, and piezoelectric coefficient, e_{33}, dropping significantly under initial 20 MPa uniaxial pressure, to the extent that the degraded piezoelectric properties are worse than those of PZT ceramics [14]. This suggests it is desirable to avoid direct pressure loading of piezocrystals when they are assembled into transducers and that the mass-spring design is not the best for piezocrystal application.

In this situation, it is useful to explore alternative designs that may take advantage of the high performance of piezocrystals. One example is a simplified approach suggested by Lal and Friedrich in which the piezoelectric drive components are directly bonded to a planar tool [15, 16]. Based on this approach, a new design utilizing the d_{31}-mode is proposed in this paper, using PMN-28%PT piezocrystal in the form of a multi-domain single crystal in the rhombohedral phase, poled along the [001] crystallographic direction [17]. Table I compares relevant parameters of PMN-28%PT with PZT4 piezoceramic [18]. As shown, the d_{31} coefficient is more than four times that of PZT4 piezoceramic and the coupling coefficient, k_{31}, is 30% higher.

TABLE I. COMPARISON OF RELEVANT PARAMETERS OF PZT4 AND [001] POLED PMN-28%PT

Parameter	PZT4	[001] poled PMN-28%PT
d_{31} (10^{-12} C/N)	-128	-569
d_{33} (10^{-12} C/N)	328	1182
k_{33}	0.68	0.91
k_{31}	0.33	0.44
s_{33}^E (10^{-12} m^2/N)	19.60	34.38
s_{11}^E (10^{-12} m^2/N)	13.00	44.57

The work here is based on the hypothesis that this significant difference in material properties can be exploited in practice in additional performance in needle-actuation transducers. An immediate objective of the work was thus to identify an alternative needle-actuation transducer design utilizing the d_{31} mode of piezoceramic and to further improve its performance by implementing it with piezocrystal. A needle actuation transducer based on the d_{33} mode was also fabricated and characterized for comparison. Section II of the paper outlines the methodology for design, simulation, fabrication and characterization. Detailed performance comparisons of the three needle actuation transducers are given in Section III and Section IV presents conclusions and suggests further work to realize devices for clinical adoption.

II. METHODOLOGY

A. Design

To utilize the d_{31} mode of piezoelectric material, a new design based on a planar tool concept is proposed here. It is a small, external, hand-held piezoelectric device which can be quickly clamped onto a standard medical needle. As shown in Fig. 1(a), four piezoelectric plates with dimensions 10 x 3 x 1 mm^3 were directly bonded to four flattened surfaces of a stepped horn-shaped hollow cylinder positioned at 90 ° circumferentially with respect to one another. A standard anaesthesia needle can be inserted and gripped by tightening a clamping cap, Fig. 1(b). The anaesthesia needle is then actuated by the device at low ultrasonic frequencies, in the range 20 – 50 kHz. This design eliminates the prestress in the mass-spring configuration which degrades the performance of piezocrystals, making it suitable for both piezocrystal and piezoceramic. Both have been utilized to obtain the results presented here.

(a)

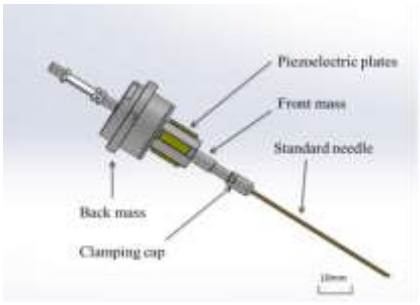

(b)

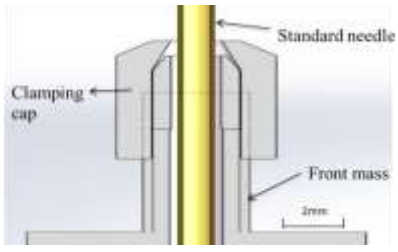

Figure 1. (a) General view of d_{31} needle actuation transducer and (b) cross sectional view of clamping cap illustrating the clamping method

The d_{33} mode transducer used for comparison is based on the mass-spring configuration. The structures and dimensions of both transducers are listed in Fig. 2 for comparison.

(a)

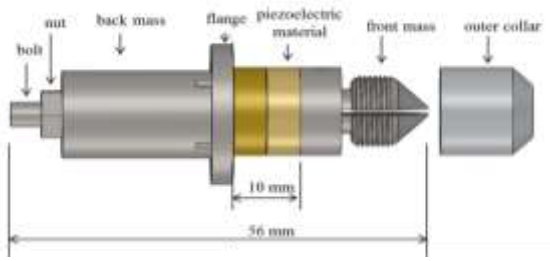

(b)

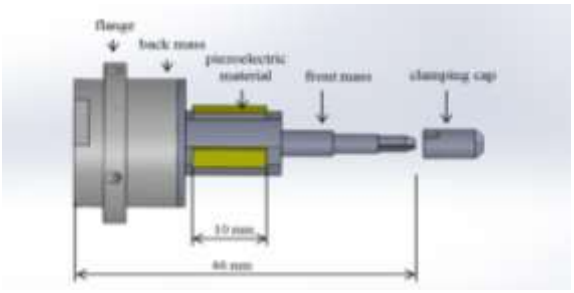

Figure 2. Structures and dimensions of the (a) d_{33}-mode transducer and (b) d_{31}-mode transducer

B. Simulation

Before fabrication, individual transducers were modelled numerically using the finite element analysis (FEA) software ABAQUS (Dassault Systèmes Simulia, Paris, France) to determine resonant frequencies and modal shapes. The properties of PZT4 (Meggitt Sensing Systems, Kvistgaard, Denmark) and [001]-orientated PMN-28%PT (Morgan Technical Ceramics, Ruabon, UK) were input for simulation, with ANSI304 stainless steel and aluminum alloy properties used for the back and front masses of the transducers, respectively.

In each experimental device, the piezoelectric plates are bonded to the front mass with Ag-loaded epoxy and the bond lines in this configuration were also included in the ABAQUS model, with the properties in Table II [19]. With the thickness of the bond line in the range 10 – 100 μm or more, it is difficult to measure accurately with a direct technique such as the use of a micrometer. However, the thickness can be estimated using the ultrasonic pulse-echo method [19]. In this way, an estimate of 40 μm was obtained and this was built into the model. The effects of wire connections were ignored.

TABLE II. MATERIAL PARAMETERS OF SILVER-LOADED EPOXY[19]

Property	Silver-loaded epoxy
Density, ρ (kg/m^3)	3.70 x 10^3
Elastic stiffness, *c* (N/m)	8.32 x 10^9
Poisson's ratio, ν	0.36

TABLE III. PIEZOELECTRIC MATERIALS USED FOR FABRICATION

Property	PZT4 d_{33} rings	PZT4 d_{31} plates	PMN-28%PT d_{31} plates
f_r(kHz)	320.37 (σ = 1.12)	160.37 (σ = 0.92)	80.86 (σ = 0.28)
f_a(kHz)	383.77 (σ = 1.26)	168.12 (σ = 1.09)	89.53 (σ = 0.26)
k_{31}	N/A	0.33 (σ = 0.0033)	0.47 (σ = 0.0022)
k_t	0.47 (σ = 0.0016)	N/A	N/A
d_{33} (10^{-12} C/N)	307 (σ = 1.08)	N/A	N/A
d_{31} (10^{-12} C/N)	N/A	-117 (σ = 1.21)	-556 (σ = 4.52)
C (nF) (at 1kHz)	0.31 (σ = 0.0083)	0.44 (σ = 0.0095)	1.25 (σ = 0.017)

* Standard deviation is reported because multiple samples were measured and used for single transducer fabrication

C. Fabrication

Before fabrication, all the piezoelectric material was checked for consistency by measuring the electrical impedance spectra and extracting relevant properties, with the results summarized in Table III.

The complete transducer manufacturing process involves sample pre-treatment, bonding and other processing. Both PZT4 and PMN-PT d_{31}-mode needle-actuation transducers were fabricated in the same way. For comparison, a d_{33}-mode needle actuation transducer with conventional mass-spring design [20, 21] was made with two PZT4 rings with outer diameter 15 mm, inner diameter 8 mm and thickness 5 mm.

The aim of pre-treatment is to clean the surfaces of the samples to maximize bonding quality. All the samples were cleaned using isopropanol (IPA) solvent followed by blow drying. During fabrication, the bonding process is of vital importance. Ag-loaded epoxy (Agar Scientific Ltd., Essex, UK) was used to establish both electrical and thermal contact between the electrodes on the d_{31} plates and the aluminum substrate. A jig, Fig. 3(a), was specially designed for alignment when bonding the piezoelectric plates to the flattened surfaces of the host cylinder. About 4MPa pressure was applied to exclude gas bubbles from the layer of Ag-loaded epoxy and should be maintained during the curing period. After bonding, Ag-loaded epoxy was also used to bond the lead wires to the surfaces of the piezoelectric plates. Electrical resistance was checked to ensure good connections were achieved. A completed device is shown in Fig. 3(b). Its weight is about 37.3g. In comparison, the weight of fabricated d_{33}-mode needle-actuating transducer is about 60.2g

(a)

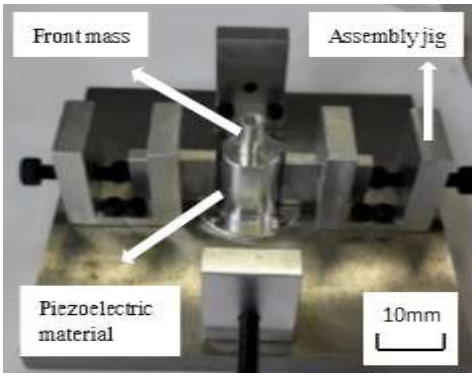

(b)

Figure 3. (a) Bespoke assembly jig and (b) completed PMN-PT d_{31}-mode transducer with needle attached

D. Characterization

Complete characterization of the fabricated devices was carried out using small and large signal characterization techniques to establish the basic and functional performance.

Small signal characterization was performed using a high resolution impedance spectroscopy measurement system in which multiple measurements over sequential frequency ranges were made with an impedance analyzer (4395A, Agilent Technologies / Keysight Technologies, Santa Rosa, CA, USA) with a limit of 801 measurement points to give a total of 24,000 points in each spectrum. This allows the performance of each device to be derived numerically with high precision.

The testing arrangement for large signal characterization is shown in Fig. 4. A PC is used to control the frequency and amplitude of a signal from a signal generator (33220A, Agilent Technologies / Keysight Technologies, Santa Rosa, CA, USA) which is applied to a power amplifier (2100L, E&I, Rochester, NY, USA). This provides sinusoidal signal for the transducer under test. For all the measurements of transducers with needle attachment, the needles were gripped at the same distance 50 mm from the tip. The voltage across the transducer and the current in the circuit are sampled with a voltage probe (N2862B, Agilent Technologies / Keysight Technologies, Santa Rosa, CA, USA) and a current probe (P602, Tektronix, Bracknell, UK) respectively. Vibration

amplitude could also be measured directly with a laser Doppler vibrometer (LDV) (OFV2570/OFV534, Polytec Ltd, London, UK). All the signals are digitized with a PXIe system (5122 / 6124, National Instruments, Newbury, UK) and analyzed by computer.

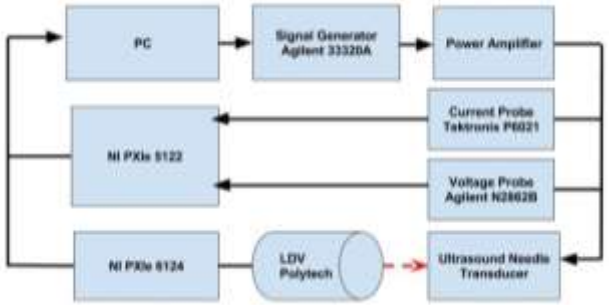

Figure 4. Diagram showing the arrangement for large signal characterization

The characterization procedures can be divided into two parts: (1) small and large signal characterization for d_{31}-mode transducers without attachment of a needle to elucidate transducer behavior; and (2) small and large signal characterization for d_{31}-mode transducers with a needle attached. For needle actuation, each device was driven at its respective needle resonant modes (NRMs) with increasing driving voltage amplitudes. The definition of NRM and the reason for driving in this mode are discussed in Section III. The LDV was used to measure displacements at different locations including the needle tip and the clamping cap. The characterization results are summarized in figures and tables in Section III.

III. Results and Discussion

A. Transducer without needle attachment

To prove the design concept of the proposed d_{31} needle actuation transducer, FEA was performed to obtain the resonant frequency and mode shape. The simulation results were then compared with the results from experimental characterization. Each of the three fabricated transducers was characterized and compared with the others.

First, each transducer was modelled without a needle attached. Two longitudinal transducer resonant modes (TRMs) were observed in the d_{31}-mode PMN-PT transducer model. The first was found at 26128 Hz with the modal shape shown in Fig. 5(a). The maximum axial vibration amplitude is located at the front of the cap where the needle will be clamped and the nodal plane is located at the flange of the back mass. The second longitudinal mode was found at 62253 Hz with the modal shape shown in Fig. 5(b). Modal analysis was also performed on the other two transducer models, with the results summarized in Table IV.

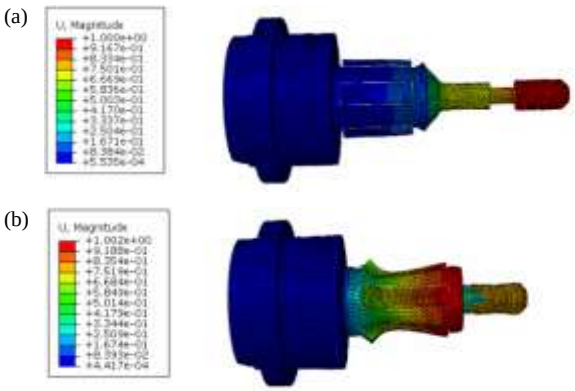

Figure 5. PMN-PT d_{31}-mode transducer mode shapes for (a) first longitudinal mode (26128 Hz) and (b) second longitudinal mode (62253 Hz)

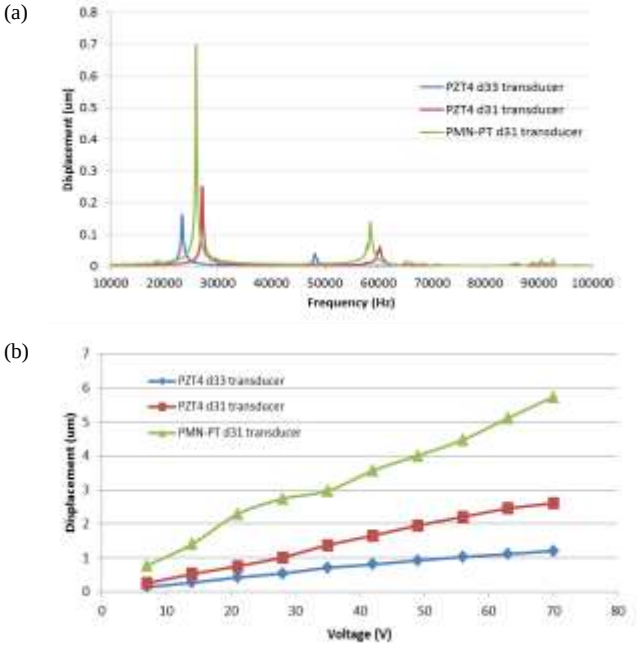

Figure 6. (a) Spectrum of axial displacement of clamping cap obtained from LDV when driving the transducers at 10 V_{pp} and (b) peak axial displacements of clamping caps measured under increasing driving voltages for each of the three transducers.

TABLE IV. Performance Comparison of three transducers. All results are for the Longitudinal mode and all results are Experimental unless indicated otherwise

	PZT4 d_{33} transducer	**PZT4 d_{31} transducer**	**PMN-PT d_{31} transducer**
1st L mode (simulation)	22208 Hz	26785 Hz	26128 Hz
1st L mode	23387 Hz	27100 Hz	25975 Hz
2nd L mode (simulation)	49286 Hz	65727 Hz	62253 Hz
2nd L mode	48250 Hz	60287 Hz	58487 Hz

Peak cap displacement at 1st L model	0.163 μm	0.251 μm	0.696 μm
Peak cap displacement at 2nd L mode	0.039 μm	0.062 μm	0.139 μm
Quality factor for 1st L mode	72	139	102
Resonance Impedance at 1st L mode	4216 Ω	3677 Ω	1329 Ω

Small and large signal characterization was carried out on all three transducers without a needle attached. A frequency sweep with 10 V_{pp} amplitude was performed to obtain the displacement spectrum of the clamping cap using the LDV. Fig. 6(a) includes the characterization result for the PMN-PT d_{31}-mode transducer. A peak axial displacement of 0.696 μm was found at 25975 Hz and the electrical impedance magnitude at this frequency was 1329 Ω. Axial displacements of the clamping cap were measured at the first longitudinal mode under increasing driving voltages up to 70 V_{pp} The other transducers were tested in the same way and the results are summarized in Fig. 6(b) and Table IV.

Comparing the frequencies of first resonance obtained from simulation and experimental tests, there are relatively small discrepancies of only several hundred Hz. These can be attributed to three effects: (1) differences between the data provided by the supplier and the actual parameters of piezoelectric material; (2) manufacturing imperfections; and most importantly (3) vibration damping caused by the use of Ag-loaded epoxy. The larger frequency difference between simulation and experimental tests observed at the second longitudinal mode may result from higher damping loss at the higher frequency.

The different configurations of transducers led to quite different resonant frequencies for the PZT4 d_{31}- and d_{33}-mode transducers. Although the same piezoceramic was used in both transducers, the PZT4 d_{31}-mode transducer had better performance than the PZT4 d_{33}-mode transducer, with higher displacement output, higher quality factor and lower resonance impedance. Compared to the nominally identical transducer made with PZT4 piezoceramic, the PMN-PT d_{31}-mode transducer produced more than double the displacement and has only about one third of the electrical impedance magnitude, attributed to the higher values of d_{31} and k_{31} shown in Table I. The lower value of electrical impedance magnitude also contributes to the improvement of mechanical performance by increasing the current in the circuit under the same drive voltage. Moreover, the higher compliance of PMN-PT resulted in a lower resonant frequency; a lower quality factor was also found. Finally, comparing all three transducers, the PMN-PT d_{31} mode transducer has the lowest electrical impedance magnitude at resonance and the highest output displacement at any given driving voltage.

B. Transducer with needle attachment

A needle was then added into each ABAQUS model and, similarly, the longitudinal modes were identified. There exist both an NRM and a TRM in the first two longitudinal modes. The NRM is termed as such because observations from simulation show that the needle is resonant at this frequency but not the transducer. However, only the transducer is resonant when vibrating at the TRM. The NRM and TRM mode shapes for the PMN-PT d_{31}-mode transducer with needle attached are shown in Fig. 7. The NRM was at 20375 Hz and the maximum displacement was found at the needle tip. The TRM shifted from 26128 Hz to 30363 Hz and the peak displacement was also found at the needle tip. The simulation results for all three transducers are summarized in Table V.

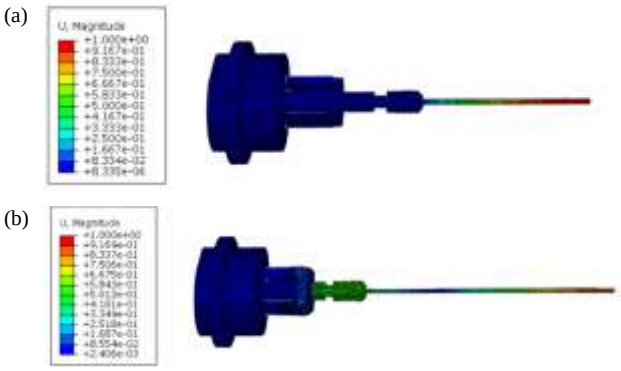

Figure 7. Mode shapes of PMN-PT d_{31}-mode transducer with needle attached (a) needle resonant mode at 20375 Hz and (b) transducer resonant mode at 30363 Hz

In Table V, a 100 mm long G21 needle was gripped at a distance 50 mm from the tip. This grip position defines the distance from the needle tip to clamping point. It allows satisfactory needle penetration into soft tissue and maintains the first NRM at an ultrasonic frequency. It has been observed that the frequency of NRM shifts when the needle is gripped at different locations [22]. To find out more about NRM shifting with the d_{31} mode transducer, simulations were performed with the grip position changed for each modal analysis. The results are summarized in Table VI. The grip position also indicates the usable length of needle, with longer usable length preferred. However, from the data in Table VI, we find that the NRM frequency decreases with the increasing value of grip position. For this reason, a distance of 50 mm from the tip was chosen as the grip position to allow maximum usable length and keep the NRM above ultrasonic frequency. Keeping the NRM above the ultrasonic frequency enables the needle to be actuated at ultrasonic frequency. Because initial tests of ultrasound actuated needle in phantom and tissue have demonstrate the feasibility of reduction of force and deflection during needle insertion [23].

TABLE V. PERFORMANCE COMPARISON OF THREE NEEDLE ACTUATION TRANSDUCERS. ALL RESULTS ARE FOR LONGITUDINAL MODES AND ALL RESULTS ARE EXPERIMENTAL UNLESS INDICATED OTHERWISE

	PZT4 d_{33} transducer with needle	**PZT4 d_{31} transducer with needle**	**PMN-PT d_{31} transducer with needle**
Needle mode (simulation)	22186 Hz	21376 Hz	20375 Hz
Needle mode	21100 Hz	20237 Hz	19900 Hz
Transducer mode (simulation)	25050 Hz	31616 Hz	30363 Hz
Transducer mode	23500 Hz	30362 Hz	29912 Hz
Impedance at NRM	7190 Ω	4959 Ω	1854 Ω
Needle tip displacement at NRM	0.504 μm	0.614 μm	1.275 μm

TABLE VI. FREQUENCY SHIFT OF NEEDLE RESONANT MODE WHEN GRIPPING AT DIFFERENT POSITIONS, SIMULATED WITH FEA MODEL OF PMN-PT DEVICE

Grip position (mm)	**Needle resonant mode (Hz)**
25	55067
30	44933
40	38771
50	20375
60	19077
70	16963
80	15168

Experimentally, the same standard G21 anaesthesia needle with a length of 100 mm was gripped by the transducers at the same position, 50 mm from the needle tip. The appearance of NRM at 19900 Hz and TRM at 29912 Hz can be observed from the displacement and impedance spectra in Fig. 8. When performing frequency sweeping at a signal amplitude of $10V_{pp}$, the peak displacement of the needle tip was 1.275 μm for NRM and 1.023 μm for TRM. Although both NRM and TRM generate maximum displacement output at the needle tip, the performance is different when driving at the two different modes. By measuring the needle tip displacement at the same driving voltages, the performance of the two modes can be compared [24]. Therefore, similar measurements were performed on PZT4 and PMN-PT d_{31}-mode transducers with the needle attached under increasing driving voltages.

According to Fig. 9, the axial needle tip displacement is positively related to increasing drive voltage for both transducers driven at both modes. For both transducers at an initial 20 V_{pp}, needle tip displacement when driving at NRM is slightly higher than at TRM but it becomes much higher at

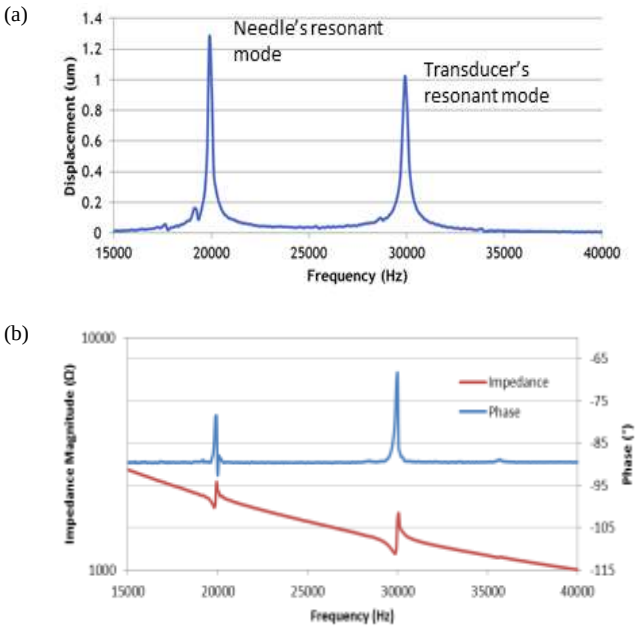

Figure 8. (a) Spectrum of axial displacement of needle tip obtained from LDV for the PMN-PT d_{31}-mode transducer driven at 10 V_{pp} and (b) impedance spectrum of PMN-PT transducer with needle attached

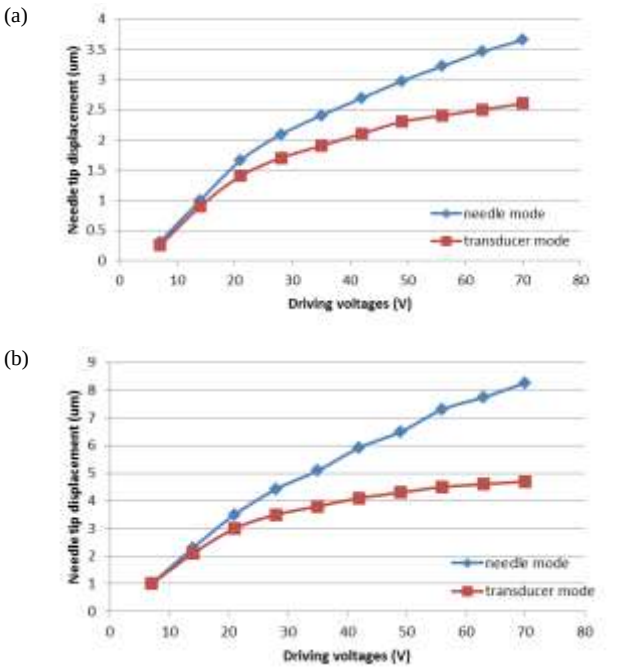

Figure 9. Axial needle tip displacement comparison between needle resonant mode and transducer resonant mode for (a) PZT4 d_{31}-mode transducer with needle attachment and (b) PMN-PT d_{31}-mode transducer with needle attachment

higher drive voltages, especially for the PMN-PT d_{31}-mode transducer. It was also observed from simulation that when the transducer is resonant at TRM, the vibrations of cap and needle are in opposite phases, which means that the needle is shortened in length at the same moment the cap reaches its maximum extended displacement. This helps explain why the needle tip has lower displacement output when driving at TRM and, as a consequence, why driving at NRM is more efficient than driving at TRM.

High drive conditions are normally required to obtain strong needle vibration during penetration into tissue [25] and the efficiency is critical under these conditions. As a consequence, all the needle actuation transducers were characterized at their respective needle resonant frequencies with drive voltages up to 70 V_{pp}. The displacements of different locations on the devices, including needle tip and clamping cap, were measured using the LDV. The results obtained were analyzed to compare the performance of the different transducers.

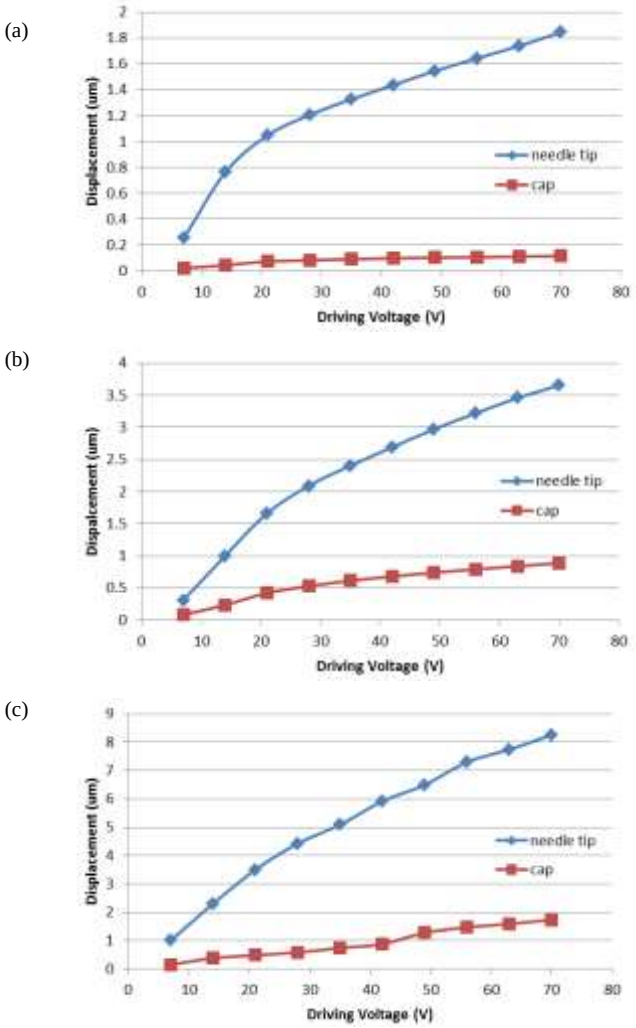

Figure 10. Peak axial displacements of needle tip and clamping cap measured at corresponding needle resonant mode for each of the three transducers (a) PZT4 d_{33} needle actuation transducer, (b) PZT4 d_{31} needle actuation transducer, (c) PMN-PT d_{31} needle actuation transducer

For each needle actuation transducer, the displacement amplitude measured at the tip of needle and the front of cap was compared under different driving conditions. As can be seen from Fig. 10, the amplitude of needle tip displacement is positively related to the drive voltage. Moreover, the needle tip shows much higher displacement than the clamping cap because the needle itself acts like a horn, amplifying the tip displacement, when driving at NRM. More specifically, the PZT4 d_{31}-mode transducer shows needle tip displacement about twice that of the PZT4 d_{33}-mode transducer when driving at the same voltage, even though the same type of piezoceramic was used as the actuation component. The PMN-PT d_{31}-mode transducer exhibits even higher output, more than four times the reference PZT4 d_{33}-mode transducer, illustrating a practical effect of the higher piezoelectric properties of PMN-PT than PZT4, as shown in Table I.

IV. CONCLUSIONS AND FUTURE WORK

Based on a proposed new transducer design to reduce mass and physical dimensions, two devices utilizing d_{31}-mode piezoceramic and piezocrystal components and one reference device utilizing d_{33}-mode piezoceramic were fabricated and tested, with the objective to compare their performance. The PZT4 d_{31}-mode device showed somewhat improved performance compared with the PZT4 d_{33}-mode device, suggesting that the new transducer design is a good alternative. Comparing all three needle actuation transducers, the d_{31}-mode device implemented with PMN-PT piezocrystal has the lowest electrical impedance and highest displacement output under the same driving voltages. This enhanced performance confirms the usefulness of piezocrystal and thus its potential to supersede traditional piezoceramics.

Future work will focus on demonstration of clinical benefits by testing the needle actuation transducers on animal tissues and soft-embalmed human cadavers [26]. Gen. III (Mn:PIN-PMN-PT) piezocrystal [27] will also be investigated to better understand the potential of piezocrystal transducers.

ACKNOWLEDGMENTS

Mr. Tingyi Jiang was supported by the China Scholarship Council and the University of Dundee. This work was also supported by the UK Engineering & Physical Sciences Research Council (EP/K020013).

REFERENCES

[1] C. D. Kelman, "Phaco-emulsification and aspiration: a new technique of cataract removal: a preliminary report," *American journal of ophthalmology*, vol. 64, pp. 23-35, 1967.

[2] S. Trenter, *et al.*, "Assessment of the ultrasonic dental scaler insert," *Medical Engineering & Physics*, vol. 24, pp. 139-144, 2002.

[3] J. E. Kennedy, *et al.*, "High intensity focused ultrasound: surgery of the future?," *British Journal of Radiology*, vol. 76, pp. 590-599, 2003.

[4] E. J. Noble, *et al.*, "Experimental comparison of mesenteric vessel sealing and thermal damage between one bipolar and two ultrasonic shears devices," *British Journal of Surgery*, vol. 98, pp. 797-800, 2011.

[5] M. R. Sadiq, *et al.*, "Enhanced US-guided needle intervention through ultrasound actuation of a standard needle," in *2014 IEEE International Ultrasonics Symposium*, 2014, pp. 827-830.

[6] M. Sadiq, "Enhanced biopsy and regional anaesthesia through ultrasound actuation of a standard needle," University of Dundee, 2013.

[7] M. P. Fronheiser, *et al.*, "Real-time 3D color flow Doppler for guidance of vibrating interventional devices," *Ultrasonic imaging*, vol. 26, pp. 173-184, 2004.

[8] T. K. Adebar, *et al.*, "3-D ultrasound-guided robotic needle steering in biological tissue," *IEEE Transactions on Biomedical Engineering*, vol. 61, pp. 2899-2910, 2014.

[9] S. Zhang, *et al.*, "Advantages and challenges of relaxor-PbTiO3 ferroelectric crystals for electroacoustic transducers – A review," *Progress in Materials Science*, vol. 68, pp. 1-66, 2015.

[10] Z. Shujun, *et al.*, "Relaxor-PbTiO³ single crystals for various applications," *IEEE Transactions on Ultrasonics, Ferroelectrics and Frequency Control*, vol. 60, pp. 1572-1580, 2013.

[11] S. Zhang and F. Li, "High performance ferroelectric relaxor-PbTiO3 single crystals: Status and perspective," *Journal of Applied Physics*, vol. 111, p. 031301, 2012.

[12] Z. Qiu, *et al.*, "Characterization of Piezocrystals for Practical Configurations With Temperature- and Pressure-Dependent Electrical Impedance Spectroscopy," *Ieee Transactions on Ultrasonics Ferroelectrics and Frequency Control*, vol. 58, pp. 1793-1803, Sep 2011.

[13] C. H. Sherman and J. L. Butler, *Transducers and arrays for underwater sound* vol. 4: Springer, 2007.

[14] X. Liao, *et al.*, "Functional Piezocrystal Characterisation under Varying Conditions," *Materials*, vol. 8, pp. 8304-8326, 2015.

[15] F. Friedrich, *et al.*, "Silicon micromachined ultrasonic transducer with improved power transfer for cutting applications," in *2012 IEEE International Ultrasonics Symposium*, 2012, pp. 1169-1172.

[16] A. Lal and R. M. White, "Silicon microfabricated horns for power ultrasonics classic," *Sensors and Actuators A: Physical*, vol. 54, pp. 542-546, 1996.

[17] T. Jiang, *et al.*, "Comparison of needle actuation transducers working in the d 31 and d 33 modes," in *Ultrasonics Symposium (IUS), 2016 IEEE International*, 2016, pp. 1-4.

[18] E. Sun and W. Cao, "Relaxor-based ferroelectric single crystals: Growth, domain engineering, characterization and applications," *Progress in Materials Science*, vol. 65, pp. 124-210, 2014.

[19] Z. Wu, "Bondlines in piezoelectric ultrasonic transducers," University of Paisley, 2005.

[20] D.-A. Wang, *et al.*, "Design of a Bézier-profile horn for high displacement amplification," *Ultrasonics*, vol. 51, pp. 148-156, 2011.

[21] X. Liao, *et al.*, "Performance optimization of ultrasonic needle actuating device for insertion operation into tissue mimics," in *Ultrasonics Symposium (IUS), 2014 IEEE International*, 2014, pp. 823-826.

[22] Y. Kuang, *et al.*, "Modelling and characterisation of a ultrasound-actuated needle for improved visibility in ultrasound-guided regional anaesthesia and tissue biopsy," *Ultrasonics*, vol. 69, pp. 38-46, 2016.

[23] X. Liao, *et al.*, "Reduced penetration force through ultrasound activation of a standard needle: An experimental and computational study," in *Ultrasonics Symposium (IUS), 2013 IEEE International*, 2013, pp. 1436-1439.

[24] Y. Kuang, "Resonance tracking and vibration stabilisation of ultrasonic surgical instruments," University of Dundee, 2014.

[25] X. Liao, "Investigation of needle-tissue interaction during ultrasonic needle intervention," University of Dundee, 2015.

[26] G. McLeod, *et al.*, "An evaluation of Thiel-embalmed cadavers for ultrasound-based regional anaesthesia training and research," *Ultrasound*, vol. 18, pp. 125-129, 2010.

[27] L. Li, *et al.*, "Enhanced dielectric, pyroelectric and ferroelectric properties of Mn-doped 0.15Pb(In1/2Nb1/2)O3–0.55Pb(Mg1/3Nb2/3)O3–0.30PbTiO3 single crystals," *Journal of Alloys and Compounds*, vol. 595, pp. 120-124, 2014.